The cellular response towards lanthanum is substrate specific and reveals a novel route for glycerol metabolism in *Pseudomonas putida* KT2440

Matthias Wehrmann[a], Maxime Toussaint[b,c], Jens Pfannstiel[d], Patrick Billard[b,c#], Janosch Klebensberger[a#]

[a]*University of Stuttgart, Institute of Biochemistry and Technical Biochemistry, Department of Technical Biochemistry, Stuttgart, Germany*

[b]*Université de Lorraine, LIEC UMR7360, Faculté des Sciences et Technologies, Vandoeuvre-lès-Nancy, France*

[c]*CNRS, LIEC UMR7360, Faculté des Sciences et Technologies, Vandoeuvre-lès-Nancy, France*

[d]*Core Facility Hohenheim, Mass Spectrometry Module, University of Hohenheim, August von Hartmann-Str. 3, 70599 Stuttgart, Germany*

Running title: Conditional responses of *Pseudomonas putida* towards rare earth elements

#Address correspondence to Janosch Klebensberger (janosch.klebensberger@itb.uni-stuttgart.de) and Patrick Billard (patrick.billard@univ-lorraine.fr)

Keywords: Lanthanides, rare earth elements, proteome, glycerol metabolism, *Pseudomonas putida*, PQQ, PedE, PedH, GarK, dehydrogenases

Abstract

Ever since the discovery of the first rare earth element (REE)-dependent enzyme, the physiological role of lanthanides has become an emerging field of research due to the potential environmental implications and biotechnological opportunities. In *Pseudomonas putida* KT2440, the two pyrroloquinoline quinone-dependent alcohol dehydrogenases (PQQ-ADHs) PedE and PedH are inversely produced in response to La^{3+}-availability. This REE-switch is orchestrated by a complex regulatory network including the PedR2/PedS2 two-component system and is important for efficient growth on several alcoholic volatiles. As *P. putida* is exposed to a broad variety of organic compounds in its natural soil habitat, the cellular responses towards La^{3+} during growth on various carbon and energy sources were investigated with a differential proteomic approach. Apart from the Ca^{2+}-dependent enzyme PedE, the differential abundance of most other identified proteins was conditional and revealed a substrate specificity. Concomitant with the proteomic changes, La^{3+} had a beneficial effect on lag-phases while causing reduced growth rates and lower optical densities in stationary phase during growth on glycerol. When these growth phenotypes were evaluated with mutant strains, a novel metabolic route for glycerol utilization was identified that seems to be functional in parallel with the main degradation pathway encoded by the *glpFKRD* operon. The newly discovered route is initiated by PedE and/or PedH, which most likely convert glycerol to glyceraldehyde. In the presence of lanthanum, glyceraldehyde seems to be further oxidized to glycerate, which, upon phosphorylation to glycerate-2-phosphate by the glycerate kinase GarK, is finally channelled into the central metabolism.

45 ## Importance

46 The biological role of rare earth elements has long been underestimated and research has mainly
47 focused on methanotrophic bacteria. We have recently demonstrated that *P. putida*, a plant growth
48 promoting bacterium that thrives in the rhizosphere of various feed crops, possesses a REE-dependent
49 alcohol dehydrogenase (PedH), but knowledge about lanthanide-dependent effects on physiological
50 traits in non-methylotrophic bacteria is still scarce. This study demonstrates that the cellular response
51 of *P. putida* KT2440 towards La^{3+} is mostly substrate specific and that during growth on glycerol, La^{3+}
52 has a severe effect on growth parameters. We provide compelling evidence that the observed
53 physiological changes are linked to the catalytic activity of PedH and thereby identify a novel route for
54 glycerol metabolism in this biotechnological relevant organism. Overall, these findings demonstrate
55 that lanthanides can alter important physiological traits of non-methylotrophic bacteria, which might
56 consequently influence their competitiveness during colonization of various environmental niches.

57 ## Introduction

58 The rhizosphere, defined as the narrow region of soil surrounding plant roots, is one of the most
59 complex ecosystems on earth containing a multitude of organisms from different taxa including fungi,
60 oomycetes, nematodes, protozoa, algae, viruses, archaea and arthropods as well as up to 10^8 soil
61 dwelling bacteria per gram of fresh root (1–3). Its diversity is mainly shaped by root exudates, a
62 complex mixture of organic compounds including carbohydrates, amino acids, or carbon acids (4, 5)
63 and plant-, fungal-, and bacteria-derived volatiles (VOCs) such as alkenes, alcohols, terpenes or
64 benzenoids (6, 7). As such, it is not surprising that the soil-dwelling organism *P. putida* KT2440 is
65 equipped with a broad diversity of metabolic pathways in order to maximize its cellular fitness in
66 different environmental niches including the rhizosphere (8–10). For efficient growth on various
67 alcoholic VOC substrates, it uses a periplasmic oxidation system consisting of the pyrroloquinoline
68 quinone-dependent alcohol dehydrogenases (PQQ-ADHs) PedE and PedH (11, 12). The enzymes
69 appear to be functionally redundant but differ in their metal cofactor dependency. PedE is a Ca^{2+}-
70 dependent enzyme, whereas PedH requires the presence of rare earth elements (REEs) of the
71 lanthanide series (Ln^{3+}) for catalytic activity (12, 13).

72 Although being among the most ubiquitous metals in the earth's crust, REEs were long considered to
73 be of no biological relevance due to their low solubility under environmental conditions (14). Indeed,
74 the only known and characterized REE-dependent enzymes thus far belong to the family of PQQ-ADHs
75 of methano- and methylotrophic bacteria as well as the non-methylotrophic organism *P. putida*
76 KT2440 (12, 15–20). A characteristic aspartic acid that is additionally present in the metal coordination
77 sphere of these enzymes is associated with Ln^{3+}-binding. Notably, this specific amino acid residue has
78 been found in the genome of many bacteria from various origins indicating a broad distribution of Ln^{3+}-
79 dependent enzymes (21–25). Very recently, another Ln^{3+}-binding protein, called lanmodulin, was
80 identified in *M. extorquens* AM1 (26). This periplasmic protein, which shows structural similarities with
81 the Ca^{2+}-binding protein calmodulin, is able to bind up to four Ln^{3+} ions per protein with picomolar
82 affinity and changes its conformation from a largely disordered to a compact, ordered state upon REE

83 binding. Although its exact cellular role has yet to be established, it has been speculated to play a role
84 in Ln^{3+}-uptake. Further, homologous genes have only been identified in the genome of some other
85 species of *Methylobacteria* and *Bradyrhizobia*.
86 In addition to their functional role as metal cofactor, several studies have recently investigated the
87 effect of REEs on cellular physiology in different methano- and methylotrophic organisms (20, 27–32).
88 Some of these studies found different physiological traits to be influenced in response to Ln^{3+}-
89 availability including changes in metabolite cross-feeding, growth rates and -yields, or biofilm
90 formation. It is further interesting to note that REEs have been used as micro-fertilizers, especially in
91 China, for over 30 years, as Ln^{3+}-supplementation can be associated with increased growth of different
92 food crops including rice, mungbean, maize, and coconut plants (33–37).
93 The aforementioned results suggest that apart from the inverse transcriptional regulation of PQQ-
94 ADHs, which has been described in detail for different organisms including *P. putida* (12, 19, 27, 38–
95 42), additional responses towards REEs exist and could depend on the specific organism and/or
96 environmental context. To investigate the existence of such conditional cellular responses in the non-
97 methylotrophic organism *P. putida* KT2440, we used a differential proteomic approach during growth
98 on various carbon and energy sources that reflect the metabolic diversity of the rhizosphere. From
99 these experiments, we found that the Ca^{2+}-dependent PQQ-ADH PedE was the only protein showing a
100 differential abundance during growth on all carbon and energy sources tested. The vast majority of
101 identified proteins were differentially abundant only under one specific growth condition. During
102 growth on glycerol and 2-phenylethanol, which both represent substrates for PedE and PedH, a
103 disproportionally high number of metabolism related proteins were more abundant in the presence of
104 La^{3+}, while this was not the case during growth on citrate and glucose, carbon and energy sources that
105 do not represent substrates for the two PQQ-ADHs. In addition, physiological characteristics, such as
106 growth rates and the lag-phase, of cultures could be linked to the differential activity pattern of PedE
107 and PedH during growth on glycerol. Based on these results, we were able to identify and reconstruct
108 a novel metabolic route for glycerol utilisation, which depends on PedE and/or PedH activity. This route
109 seems to operate in conjunction with the previously described major degradation pathway initiated

110 by the glycerol kinase GlpK and most likely ensures efficient growth of *P. putida* on this polyol

111 substrate.

112 ## Materials and Methods

113 *Bacterial strains, plasmids and culture conditions*

114 A complete list of all strains, plasmids, and primers used in this study can be found in **Table S1** and
115 **Table S2**. All *Pseudomonas putida* and *Escherichia coli* strains were maintained on solidified LB medium
116 (43). If necessary, 40 µg/mL kanamycin or 20 µg/mL 5-fluorouracil were added for maintenance and/or
117 selection. For growth, liquid LB medium or a modified M9 salt medium (12) supplemented with 5 mM
118 2-phenylethanol, 25 mM succinate, 10 mM glucose, 10 mM citrate, 20 mM DL-glycerate, or 20 mM
119 glycerol as sole source of carbon and energy was used. If not stated otherwise, precultures were grown
120 overnight in test tubes with 3 ml M9 medium supplemented with succinate at 30°C and 180 rpm. The
121 next day, cells were washed twice with M9 medium without supplemented C-source, and used to
122 inoculate 200 µL of M9 medium supplemented with the desired C-source in a 96-well microtiter plate
123 (Falcon, product no. 353047 or Sarstedt, product no. 83.3924) and incubated at 30°C and 250 rpm in a
124 microplate reader (Xenius, Safas Monaco) or 28°C and 220 rpm in a rotary shaker (Forma, Thermo
125 Scientific). Maximum growth rates (μ_{max}) and lag-times (λ) were estimated based on fitting the natural
126 logarithm of the relative OD_{600} values ($\ln(N/N_0)$, with N being OD_{600} at time t) with the Richards growth
127 model using the "grofit" package in R (44). As OD_{600} decreased directly upon begin of the experiment,
128 $\ln(N/N_{t = 3 h})$ was used instead of $\ln(N/N_0)$ for better fit. Differences in lag-times, growth rates, and
129 maximal OD_{600} during stationary phase (OD_{600}^{max}) were evaluated by statistical analysis in GraphPad
130 PRISM using a two-tailed *t*-test ($\alpha = 0.05$, $n = 3$).

131

132 *Construction of plasmids*

133 Deletion plasmids pJOE-calA, pJOE-garK, pJOE-glp, and pMW08 were constructed as follows: the 650-
134 bp to 1000-bp regions upstream and downstream of the *calA* (PP_2426), *garK* (PP_3178), *glpFKRD*
135 (PP_1076 to PP_1973), or *glcDEF* (PP_3745 to PP_3747) genes were amplified from genomic DNA of *P.*
136 *putida* KT2440 using primers PcalA1 to PcalA4, PgarK1 to PgarK4, Pglp1 to Pglp4, or MWH03 to MWH06

137 (**Table S2**). The two up- and downstream fragments and BamHI-digested pJOE6261.2 were then joined
138 together using one-step isothermal assembly (45).
139
140 *Strain constructions*
141 Deletion mutant strains were constructed as previously described (46). Briefly, the integration vector
142 pJOE6261.2 harbouring the up- and downstream regions of the target gene(s) was transformed into *P.*
143 *putida* KT2440 *Δupp* (KT2440*). Kanamycin (Kan) resistant and 5-fluorouracil (5-FU) sensitive clones
144 were selected and one of these was incubated in LB medium at 30°C for 24 h. The cell suspension was
145 then plated on M9 minimal agar plates containing 25 mM succinate and 20 µg ml^{-1} 5-FU. Clones that
146 carried the desired gene deletion were identified by colony PCR of the 5-FU^r Kan^s clones using primer
147 pair PcalA1/PcalA4, PgarK1/PgarK4, Pglp1/Pglp4, or MWH03/MWH06.
148
149 *Protein extraction for comparative proteome analysis*
150 For comparative proteome analysis experiments, 50 ml M9 medium supplemented with citrate,
151 glucose, glycerol or 2-phenylethanol and 0 or 10 µM $LaCl_3$ were inoculated with an OD_{600} of 0.05 from
152 succinate precultures of strain *P. putida* KT2440* in 250 ml polycarbonate Erlenmeyer flasks and
153 incubated at 30°C and 180 rpm. When cell cultures reached an OD_{600} of > 0.4, cells were harvested by
154 centrifugation for 15 min at 6000 x g and 4°C. Cell pellets were resuspended in 1 ml sample buffer (150
155 mM Tris-HCl pH 6.8; 2 % SDS; 20 mM dithiothreitol) and heated for 5 min at 95°C with gentle shaking.
156 Subsequently, samples were centrifuged for 15 min at 21000 x g and 4°C, and the supernatants were
157 stored in new reaction tubes at -20 °C. In a next step, proteins were precipitated using chloroform-
158 methanol (47) and pellets were resuspended in Tris-buffered (50 mM, pH 8.5) urea (6 M). Protein
159 concentrations were determined by the Bradford assay (48).
160
161 *In-solution digest of proteins and peptide purification with C18 Stage Tips*
162 To 25 µg protein in 60 µl Tris-buffered (50 mM, pH 8.5) urea (6 M), DTT was added to a final
163 concentration of 10 mM to guarantee reduction of cysteines. Samples were incubated for 30 min at

164 56 °C under shaking at 1000 rpm. Alkylation of cysteines was performed by adding 30 mM
165 iodoacetamide and incubation for 45 min at room temperature in the dark. Alkylation was stopped by
166 adding 50 mM DTT and samples were incubated for another 10 min at RT. 500 ng LysC protease (Roche)
167 in 50 mM Tris buffer (pH 8.5) was added and samples were digested overnight at 30 °C. Next, the urea
168 in the reaction mixture was diluted to 2 M by adding the appropriate amount of Tris buffer (50 mM,
169 pH 8.5). 1 µg trypsin (Roche) in Tris buffer (50 mM, pH 8.5) was added and digestion was continued for
170 4 hours at 37 °C. The digest was stopped by addition of 3 µl 10% (v/v) trifluoroacetic acid (TFA). Next,
171 peptide mixtures were concentrated and desalted on C18 stage tips (49) and dried under vacuum.
172 Samples were dissolved in 20 µl 0.1% (v/v) TFA. Aliquots of 1 µl were subjected to nanoLC-MS/MS
173 analysis.
174
175 *Mass spectrometry analysis*
176 NanoLC-ESI-MS/MS experiments were performed on an EASY-nLC 1200 system (Thermo Fisher
177 Scientific) coupled to a Q-Exactive Plus mass spectrometer (Thermo Fisher Scientific) using an EASY-
178 Spray nanoelectrospray ion source (Thermo Fisher Scientific). Tryptic peptides were directly injected
179 to an EASY-Spray analytical column (2 µm, 100 Å PepMapRSLC C18, 25 cm × 75 µm, Thermo Fisher
180 Scientific) operated at constant temperature of 35 °C. Peptides were separated at a flow rate of 250
181 nL/min using a 240 min gradient with the following profile: 2% - 10% solvent B in 100 min, 10% - 22%
182 solvent B in 80 min, 22% - 45% solvent B in 55 min, 45% - 95% solvent B in 5 min and isocratic at 90%
183 solvent B for 15 min. Solvents used were 0.5 % acetic acid (solvent A) and 0.5% acetic acid in
184 acetonitrile/H2O (80/20, v/v, solvent B). The Q Exactive Plus was operated under the control of
185 XCalibur 3.0.63 software. MS spectra (m/z = 300-1600) were detected in the Orbitrap at a resolution
186 of 70000 (m/z = 200) using a maximum injection time (MIT) of 100 ms and an automatic gain control
187 (AGC) value of 1 x 10^6. Internal calibration of the Orbitrap analyzer was performed using lock-mass ions
188 from ambient air as described elsewhere (50). Data dependent MS/MS spectra were generated for the
189 10 most abundant peptide precursors in the Orbitrap using high energy collision dissociation (HCD)
190 fragmentation at a resolution of 17500, a normalized collision energy of 27 and an intensity threshold

191 of 1.3 x 10^5. Only ions with charge states from +2 to +5 were selected for fragmentation using an
192 isolation width of 1.6 Da. For each MS/MS scan, the AGC was set at 5 x 10^5 and the MIT was 100 ms.
193 Fragmented precursor ions were dynamically excluded for 30 s within a 5 ppm mass window to avoid
194 repeated fragmentation.
195
196 *Protein quantification and data analysis*
197 Raw files were imported into MaxQuant (51) version 1.6.0.1 for protein identification and label-free
198 quantification (LFQ) of proteins. Protein identification in MaxQuant was performed using the database
199 search engine Andromeda (52). MS spectra and MS/MS spectra were searched against *P. putida*
200 KT2440 protein sequence database downloaded from UniProt (53). Reversed sequences as decoy
201 database and common contaminant sequences were added automatically by MaxQuant. Mass
202 tolerances of 4.5 ppm (parts per million) for MS spectra and 20 ppm for MS/MS spectra were used.
203 Trypsin was specified as enzyme and two missed cleavages were allowed. Carbamidomethylation of
204 cysteines was set as a fixed modification and protein N-terminal acetylation and oxidation were
205 allowed as variable modifications. The 'match between runs' feature of MaxQuant was enabled with
206 a match time window of one minute and an alignment time window of 20 minutes. Peptide false
207 discovery rate (FDR) and protein FDR thresholds were set to 0.01.
208 Statistical analysis including *t*-tests and principal component analysis (PCA) were performed using
209 Perseus software version 1.6.0.2 (54). Matches to contaminant (e.g., keratins, trypsin) and reverse
210 databases identified by MaxQuant were excluded from further analysis. Proteins were considered for
211 LFQ (label free quantification) if they were identified by at least two peptides. First, normalized LFQ
212 values from MaxQuant were log2 transformed. Missing values were replaced from normal distribution
213 using a width of 0.2 and a downshift of 2.0. Statistical differences between two sample groups were
214 determined using an unpaired *t*-test and a p-value < 0.01 and a regulation factor > 2 (log2 fold-change
215 > 1) were considered as significant change in protein abundance. The mass spectrometry proteomics
216 data will be deposited to the ProteomeXchange Consortium via the PRIDE (55) partner repository
217 (submitted).

218

219 *Purification and activity measurement of PQQ-ADHs PedE and PedH*

220 To measure the activity of the two PQQ-ADHs PedE and PedH, the enzymes were expressed in *E. coli*
221 BL21(DE3) cells using plasmids pMW09 and pMW10, and purified by affinity chromatography as
222 described elsewhere (12). The activities with the four substrates 2-phenylethanol, citrate, glucose and
223 glycerol were determined at a concentration of 10 mM using a previously described colorimetric assay
224 (12) with one minor modification. To represent the growth conditions, 1 µM La^{3+} instead of 1 µM Pr^{3+}
225 was used as metal cofactor for PedH.

226 ## Results

227 We have recently demonstrated that the two PQQ-ADHs PedE and PedH are inversely regulated
228 dependent on the presence of rare earth elements (REEs) and that a complex signalling network, which
229 includes the activity of the PedR2/PedS2 two-component system, orchestrates this regulation (12, 38).
230 To identify whether a global cellular response of *P. putida* KT2440 towards REEs beyond the regulation
231 of the PQQ-ADHs exists, we used a comparative proteomic analysis during growth on four different
232 carbon and energy sources, namely 2-phenylethanol, glycerol, glucose, and citrate.

233

234 *Evaluation of proteomics data*

235 Proteins were extracted from cells of *P. putida* by SDS to enable extraction of cytoplasmic as well as
236 transmembrane proteins followed by label free nano-LC-MS/MS quantification. In total, 2771 proteins
237 with at least two unique peptides and an FDR ≤ 1% were identified and quantified by our proteomics
238 approach, corresponding to approximately 50% of the *P. putida* KT2440 proteome. Principal
239 component analysis revealed high reproducibility for sample replicates and distinct patterns for the
240 different carbon sources (**Fig. S1**). The majority of proteins was increased or decreased in abundance
241 in response to the different carbon and energy sources. In contrast, minor differences were observed
242 in the presence or absence of La^{3+} during growth on the same carbon and energy source. Proteins that
243 exhibited a 2-fold or higher change in abundance between different growth conditions and a *p*-value
244 ≤ 0.01 were considered as differentially abundant.

245

246 *Effect of lanthanum on protein abundance during growth with different substrates*

247 According to the aforementioned criteria, 56 proteins were identified as differentially abundant
248 comparing growing cells of *P. putida* in the presence and absence of La^{3+} with different carbon sources
249 (**Fig. 1, Table 3, Table S3-S5**). In these studies, only the Ca^{2+}-dependent PQQ-ADH PedE (PP_2674)
250 showed a decreased abundance in response to La^{3+} during growth on all four different carbon and
251 energy sources. The Ln^{3+}-dependent PQQ-ADH PedH (PP_2679) showed an increased abundance in

252 response to La^{3+} during growth on glucose, glycerol, and 2-phenylethanol, whereas an uncharacterized
253 pentapeptide repeat containing protein (PP_2673) that is directly upstream of *pedE* showed a
254 decreased abundance during growth on glycerol and 2-phenylethanol (**Fig. 1**). The remaining 53
255 proteins were only identified under one specific growth condition (**Table 3, Table S3-S5**).
256 During growth on 2-phenylethanol and glycerol, a majority of the identified proteins was increased in
257 abundance (80% and 70%) in response to La^{3+} (**Table 3, Table S3**). For glucose and citrate this was
258 different, as most of the identified proteins were found to be less abundant in response to La^{3+} (36%
259 and 40% during growth on glucose and citrate; **Table S4 and Table S5**). Notably, the majority of the
260 identified proteins were related to metabolism according to the cluster of orthologous protein groups
261 (COG) database (56). To test whether the observed conditional proteomic response is linked to PedE
262 and/or PedH activity, we determined the corresponding enzyme activities with all four carbon and
263 energy sources (**Table 1**). Apart from the already known substrate 2-phenylethanol, PedE and PedH
264 also showed activity with glycerol, whereas no activity could be detected with citrate or glucose.
265
266 *Effect of lanthanum during growth on glycerol*
267 From our proteomic- and biochemical data, we speculated that PedE and PedH activity could play a
268 beneficial role during glycerol metabolism of *P. putida* KT2440. As the degradation pathway and
269 growth characteristics of this organism have been recently characterized in great detail (57, 58), we
270 wanted to have a closer look on the effect of La^{3+} during growth on this specific carbon and energy
271 source. In these experiments (**Fig. 2A, Table 2)**, we consistently observed a shorter lag-phase (λ) of the
272 cultures in response to La^{3+}-availability (10.2 ± 0.2 h vs. 17.3 ± 0.2). Additionally, the corresponding
273 values of the specific growth rates (μ_{max}, 0.201 ± 0.004 vs. 0.341 ± 0.010 h^{-1}) and the maximal OD_{600} in
274 stationary phase (OD_{600}^{max}; 0.680 ± 0.014 vs. 0.884 ± 0.004) of the cultures differed in the presence or
275 absence of La^{3+}, respectively. As the purified PedH enzyme showed a 3-fold higher specific activity
276 towards glycerol compared to PedE *in vitro* (0.9 ± 0.1 U mg^{-1} vs. 0.3 ± 0.1 U mg^{-1}; **Table 1**), we
277 speculated that this increased glycerol conversion by PedH could be the underlying cause for the
278 observed differences in growth parameters. When subsequently a Δ*pedE* Δ*pedH* strain was analysed

279 for growth in the presence and absence of La^{3+} (**Fig. 2B**, **Table 2**), no significant differences in λ and
280 μ_{max} were observed for the Δ*pedE* Δ*pedH* strain in response to La^{3+} while, although less profound, small
281 differences in OD_{600}^{max} were still detected. Further, under both conditions the double deletion strain
282 showed a lag-phase that was undistinguishable from that of the parental strain in the absence of La^{3+}
283 but dramatically longer than that of the parental strain in the presence of La^{3+} (17.5 ± 0.3 h in the
284 absence of La^{3+} and 17.2 ± 0.4 h in the presence of 10 µM La^{3+}). Interestingly, the growth rates under
285 both conditions (0.276 ± 0.008 h^{-1} and 0.291 ± 0.012 h^{-1}) were significantly higher ($p < 0.01$) than those
286 of the parental strain in presence of La^{3+} while still being significantly below ($p < 0.05$) those of the
287 parental strain in the absence of La^{3+}.
288 These results implied that the two PQQ-ADHs can indeed be beneficial for growth on glycerol and that
289 a functionally active PedH enzyme is the underlying cause for the La^{3+}-dependent differences in lag-
290 times and growth rates and to some extent also for differences in OD_{600}^{max} of KT2440 cultures. As PedE
291 and PedH as well as the remaining proteins that were found to be differentially abundant in response
292 to La^{3+} during growth on glycerol, are not part of the described degradation pathway in *P. putida*
293 KT2440 (57, 58), we hypothesized that an additional metabolic route exists (**Fig. 3**). Based on our
294 proteomic data, this route could be initiated by the activity of PedH and the oxidation of glycerol to
295 glycolaldehyde. In the next steps glycolaldehyde could be oxidized to glycerate by PedH, the aldehyde
296 dehydrogenase AldB-II, or the aldehyde oxidase complex composed of proteins PP_3621 (IorA-II),
297 PP_3622 and PP_3623 (AdhB). After phosphorylation by the glycerate kinase GarK, glycerate-2-
298 phosphate could eventually enter the central metabolism.
299 If such a metabolic route exists, a Δ*glpFKRD* deletion strain should still be able to grow with glycerol as
300 sole source of carbon and energy, whereas a Δ*pedE* Δ*pedH* Δ*glpFKRD* deletion mutant should not. To
301 test this scenario, the corresponding strains were constructed and characterized for their growth
302 phenotypes (**Fig. 4A**). We found that *P. putida* KT2440 indeed grew on glycerol independent of the
303 GlpFKRD pathway, although growth was dramatically impaired compared to the parental strain or
304 strain Δ*pedE* Δ*pedH*. When PedE and PedH were additionally deleted, no growth was observed even
305 after a prolonged incubation time of 5 d. This supported our hypothesis that a metabolic route for

306 glycerol next to the GlpFKRD pathway exists and that this route is initiated by PedE and PedH, most
307 likely by the oxidation of glycerol to glyceraldehyde (**Fig. 3**). Given that the route further proceeds *via*
308 glycerate and glycerate-2-phosphate, different cellular concentrations of these metabolites would be
309 expected during growth on glycerol in a mutant that is not able to use the GlpFKRD pathway.
310 Interestingly, a companion study to this work employed a metabolome analysis using glycerol-growing
311 cells of *P. putida* KT2440 and a Δ*glpK* deletion strain, which can only use the proposed novel route *via*
312 PedE and PedH (59). In their experiments, the authors observed that the glycerate concentration
313 measured for the Δ*glpK* strain was dramatically increased compared to the wild type, whereas
314 concentrations of glyceraldehyde and glyceraldehyde-3-phosphate were in the same range for both
315 strains. These data suggested that glycerate is indeed an intermediate during *glpFKRD*-independent
316 growth, and that the activity of downstream proteins represent the bottleneck of the metabolic route
317 leading to the observed accumulation. As our proteomic data indicated the involvement of the
318 predicted glycerate kinase GarK, we constructed a Δ*garK* deletion strain and speculated that this strain
319 should lack the ability to phosphorylate glycerate and would hence be incapable of channelling
320 glycerate-2-phosphate into the central metabolism. We indeed observed no growth of a Δ*garK* mutant
321 on glycerate even after incubation of up to 5 d, while strain Δ*pedE* Δ*pedH* Δ*glpFKRD* could grow and
322 reached OD_{600}^{max} within 72 h of incubation under the condition tested (**Fig. 4B**).
323 When grown on glycerol, no significant effect on growth rates and lag-times as well as only a minor,
324 but significant, negative effect on the OD_{600}^{max} ($p < 0.01$) was observed for the Δ*garK* deletion in the
325 absence of La^{3+}. In contrast, the same deletion caused a dramatic growth impairment in the presence
326 of La^{3+} (**Fig. 5A**, **Table 2**) and consequently the stationary phase was not reached during the 40 h of
327 incubation. Hence, no reliable growth parameter could be deduced from these data. It is however
328 obvious that the growth rate was far below the one of the parental strain in the presence of La^{3+}.
329 Notably, some of the most severely upregulated proteins in response to La^{3+} are either related to
330 stress, namely the multidrug efflux pump MexEF and the alkylhydroperoxide reductase subunits AhpC
331 and AhpF, or are enzymes that play no obvious roles within the proposed metabolic route such as CalA,
332 a predicted coniferyl alcohol dehydrogenase, and the glycolate oxidase GlcDEF. To investigate the

333 potential influence of the latter two enzymes, we constructed and analysed the corresponding Δ*calA*
334 and Δ*glcDEF* mutants and tested their growth pattern with glycerol (**Fig. 5B; Table 2**). The Δ*glcDEF*
335 mutant showed a growth behaviour similar to the parental strain. In contrast, the Δ*calA* strain
336 exhibited a significantly increased growth rate ($p < 0.01$) and higher OD_{600}^{max} ($p < 0.01$) than the
337 parental strain in the presence of La^{3+} while showing no significant differences in OD_{600}^{max} and maximal
338 growth rate and only minor differences ($p < 0.05$) in lag-times in the absence of La^{3+} (**Fig. 5C; Table 2**).

339 ## Discussion

340 In the present study, the cellular responses of *P. putida* KT2440 towards La^{3+}-availability during growth
341 on several carbon and energy sources were investigated. The only protein that showed a differential
342 abundance independent of the substrate used for growth was the Ca^{2+}-dependent PQQ-ADH PedE.
343 This result is in line with data from a previous study (38), which demonstrated that the La^{3+}-induced
344 downregulation of *pedE* is dependent on the PedS2/PedR2 two-component system that, based on our
345 current observation, seems to be functional under all tested conditions. The other two proteins that
346 showed differential abundance under more than one culture condition (PedH, PP_2673) are both also
347 part of the *ped* gene cluster. Notably, the carbon and energy sources under which these proteins were
348 identified either represent substrates of PedE and PedH, or can be converted by an enzyme that
349 depends on the same PQQ-cofactor, namely the glucose dehydrogenase Gcd. The remaining 53
350 proteins that showed differential abundance in response to La^{3+} were identified only during growth on
351 one specific carbon and energy source, suggesting a conditional regulation. For glycerol, we provide
352 striking evidence that the increased activity of PedH compared to PedE is the primary cause for the
353 observed proteomic and physiological changes during growth.
354 Thus far, the degradation of glycerol was described to start by the uptake *via* GlpF, phosphorylation by
355 GlpK, and subsequent GlpD-catalysed oxidation of glycerol-3-phosphate to dihydroxyacetone-3-
356 phosphate (58). In a next step, dihydroxyacetone-3-phosphate is interconverted to glyceraldehyde-3-
357 phosphate and enters the central metabolism. This pathway is negatively regulated by the
358 transcriptional regulator GlpR, and the de-repression of the *glpFKRD* operon is believed to depend on
359 the intracellular concentration of glycerol-3-phosphate, which finally impacts the lag-phase of cultures
360 (57). As such, it was interesting to find that growth on glycerol in the presence of La^{3+} led to a shorter
361 lag phase and lower growth rate of the parent strain, and that a Δ*pedE* Δ*pedH* mutant showed a lag-
362 phase similar to the parent in absence of La^{3+} without any beneficial effect of La^{3+} while still growing
363 with a higher growth rate than the parent strain in presence of La^{3+}. Further experiments revealed that
364 a Δ*glpFKRD* deletion strain is still able to grow on glycerol, while a Δ*pedE* Δ*pedH* Δ*glpFKRD* is not.

365 Together with the notion that a Δ*garK* mutant cannot utilize glycerate, this strongly indicates the
366 existence of a novel route for glycerol metabolism, in which PedE and PedH catalyse the initial
367 oxidation of glycerol to glyceraldehyde. In the presence of La^{3+}, the route seems to proceed *via* a
368 second oxidation step to glycerate, which is subsequently converted to glycerate-2-phosphate by the
369 activity of GarK (**Fig. 3**). The PedE/PedH-dependent route, despite being important for efficient growth,
370 clearly is not the main route for glycerol metabolism, as the effect of the Δ*pedE* Δ*pedH* deletion on the
371 lag-phase with glycerol is far less severe than deletion of the *glpFKRD* gene cluster. It also appears that
372 the PedE/PedH-dependent route is less efficient than the GlpFKRD pathway, as the overall growth of
373 the Δ*glpFKRD* strain is substantially impaired in comparison to the Δ*pedE* Δ*pedH* strain.
374 A possible explanation could be the formation of the toxic intermediate glyceraldehyde, which is
375 known for its protein crosslinking properties and the formation of superoxide radicals due to auto-
376 oxidation (60, 61). The observed differences in growth rates and OD_{600}^{max} in response to La^{3+} in the
377 parent strain could thus reflect the increased metabolic flux towards glyceraldehyde due to the higher
378 specific activity of PedH compared to PedE. This would also explain the severe La^{3+}-dependent growth
379 impairment of the Δ*garK* mutant, as one can assume that even higher concentrations of
380 glyceraldehyde accumulate in a mutant that cannot process glycerate. The notion that the MexEF RND-
381 type transporter proteins, which are involved in efflux of various toxic compounds (62), and the
382 alkylhydroperoxide reductase subunits AhpC and AhpF, which have been linked to ROS detoxification
383 in *P. putida* (63), were also more abundant in presence of La^{3+} during growth on glycerol are supportive
384 of such a hypothesis.
385 To explain the impact of La^{3+} on the lag-times of cultures, one could speculate that in addition to
386 glycerol-3-phosphate, also other phosphorylated derivatives, such as glycerate-2-phosphate, are able
387 to relieve the repression of *glpFKRD* by GlpR. However, as in the absence of La^{3+} the growth phenotype
388 of the Δ*garK* mutant is indistinguishable from that of the parental strain, and since the growth rate of
389 the parent strain in absence of La^{3+} is still significantly higher than the growth rate of strain Δ*pedE*
390 Δ*pedH,* we postulate that yet another metabolic route is present that contributes to growth without
391 affecting the lag-phase. This second route could proceed *via* the phosphorylation of glyceraldehyde to

392 glyceraldehyde-3-phosphate by the activity of a so-far unknown kinase. Whether both alternative
393 routes to the GlpFKRD pathway are functional in parallel or whether the metabolic flux *via* glycerate is
394 exclusively induced in the presence of La^{3+} is currently unknown and would need to be tested in future
395 studies. Similarly, the question why proteins that cannot be associated to the newly discovered routes
396 for glycerol are among the most differentially abundant proteins in response to La^{3+} remains to be
397 elucidated. It is however worthwhile noting that CalA and GlcDEF are either known (GlcDEF) or
398 predicted (CalA) by the PROSITE software tool (https://prosite.expasy.org/) (64) to be catalytically
399 active on 2-hydroxy acids. As such, potential activities towards pathway intermediates such as
400 glycerate cannot be excluded at the moment.
401 From our data, the La^{3+}-dependent proteomic and physiological changes during growth on glycerol can
402 be explained by a shift in metabolic flux resulting from the differences in specific catalytic activities
403 between PedH and PedE. A similar metabolic-driven interpretation can also be used to explain the
404 proteomic differences during growth on other carbon and energy sources that are known to be
405 substrates for PedE and PedH such as 2-phenylethanol. However, this logic fails to explain the
406 differences observed during growth on glucose and citrate, as they do not represent substrates for
407 PedE and/or PedH. Despite the fact that we currently do not know the underlying cause for the
408 conditional proteomic changes under these conditions, it indicates the presence of additional effects
409 of REEs beside the interaction with PedH and PedS2/PedR2. Such effects could include the inhibition
410 of protein functions by mismetallation (65, 66), changes in the physiology of the outer membrane (67),
411 or so far unknown REE-dependent enzymes and regulator proteins. The latter explanation is of
412 particular interest, as two recent studies provide strong evidence that specific importers that can
413 transport Ln^{3+} into the cytoplasm of methylotrophic bacteria do exist (41, 68).
414 Altogether, the current study demonstrates that the utilization of REEs can influence important
415 physiological traits of *P. putida*, which could be highly beneficial in competitive environmental niches
416 such as the rhizosphere. The previously reported fertilizing effect of REEs on different food crops could
417 hence be partially the result of increased competitiveness of plant growth promoting organisms such
418 as *P. putida* during root colonization. This hypothesis is further supported by a recent study, which

419 found that Pseudomonads predominantly thrive on root exudates *in vivo* and are hence enriched in
420 the rhizosphere of *Arabidopsis thaliana* (10). As such, it will be interesting to see what future research
421 will add to the currently emerging theme of REEs being an important micronutrient for methylotrophic
422 and non-methylotrophic organisms.

423 **Reference**

424 1. Mendes R, Garbeva P, Raaijmakers J. 2013. The rhizosphere microbiome: significance of plant
425 beneficial, plant pathogenic, and human pathogenic microorganisms. FEMS Microbiol Rev
426 37:634–663.

427 2. Raaijmakers J, Paulitz TC, Steinberg C, Alabouvette C, Moënne-Loccoz Y. 2009. The rhizosphere:
428 a playground and battlefield for soilborne pathogens and beneficial microorganisms. Plant Soil
429 321:341–361.

430 3. Berg G, Roskot N, Steidle A, Eberl L, Zock A, Smalla K. 2002. Plant-Dependent Genotypic and
431 Phenotypic Diversity of Antagonistic Rhizobacteria Isolated from Different *Verticillium* Host
432 Plants Plants. Appl Environ Microbiol 68:3328–3338.

433 4. Carvalhais LC, Dennis PG, Fedoseyenko D, Hajirezaei MR, Borriss R, Von Wirén N. 2011. Root
434 exudation of sugars, amino acids, and organic acids by maize as affected by nitrogen,
435 phosphorus, potassium, and iron deficiency. J Plant Nutr Soil Sci 174:3–11.

436 5. Dakora FD, Phillips DA. 2002. Root exudates as mediators of mineral acquisition in low-nutrient
437 environments. Plant Soil 245:35–47.

438 6. Schmidt R, Cordovez V, de Boer W, Raaijmakers J, Garbeva P. 2015. Volatile affairs in microbial
439 interactions. ISME J 9:2329–2335.

440 7. Insam H, Seewald MSA. 2010. Volatile organic compounds (VOCs) in soils. Biol Fertil Soils
441 46:199–213.

442 8. Wackett LP. 2003. *Pseudomonas putida*—a versatile biocatalyst. Nat Biotechnol 21:136–138.

443 9. Nelson KE, Weinel C, Paulsen IT, Dodson RJ, Hilbert H, Martins dos Santos VAP, Fouts DE, Gill
444 SR, Pop M, Holmes M, Brinkac L, Beanan M, DeBoy RT, Daugherty S, Kolonay J, Madupu R,
445 Nelson W, White O, Peterson J, Khouri H, Hance I, Lee PC, Holtzapple E, Scanlan D, Tran K,
446 Moazzez A, Utterback T, Rizzo M, Lee K, Kosack D, Moestl D, Wedler H, Lauber J, Stjepandic D,
447 Hoheisel J, Straetz M, Heim S, Kiewitz C, Eisen J, Timmis KN, Dusterhoft A, Tummler B, Fraser
448 CM. 2002. Complete genome sequence and comparative analysis of the metabolically versatile
449 *Pseudomonas putida* KT2440. Environ Microbiol 4:799–808.

450 10. Worsley SF, Macey MC, Newitt JT, Patrick E, Yu DW, Wilkinson B, Murrell C, Hutchings MI. 2019.
451 Investigating the role of exudates in recruiting Streptomyces bacteria to the *Arabidopsis*
452 *thaliana* root microbiome. bioRxiv 532309.
453 11. Mückschel B, Simon O, Klebensberger J, Graf N, Rosche B, Altenbuchner J, Pfannstiel J, Huber
454 A, Hauer B. 2012. Ethylene glycol metabolism by *Pseudomonas putida*. Appl Environ Microbiol
455 78:8531–9.
456 12. Wehrmann M, Billard P, Martin-Meriadec A, Zegeye A, Klebensberger J. 2017. Functional Role
457 of Lanthanides in Enzymatic Activity and Transcriptional Regulation of Pyrroloquinoline
458 Quinone-Dependent Alcohol Dehydrogenases in *Pseudomonas putida* KT2440. MBio 8:e00570-
459 17.
460 13. Takeda K, Matsumura H, Ishida T, Samejima M, Igarashi K, Nakamura N, Ohno H. 2013. The two-
461 step electrochemical oxidation of alcohols using a novel recombinant PQQ alcohol
462 dehydrogenase as a catalyst for a bioanode. Bioelectrochemistry 94:75–78.
463 14. Firsching FH, Brune SN. 1991. Solubility products of the trivalent rare-earth phosphates. J Chem
464 Eng Data 36:93–95.
465 15. Pol A, Barends TRM, Dietl A, Khadem AF, Eygensteyn J, Jetten MSM, Op den Camp HJM. 2014.
466 Rare earth metals are essential for methanotrophic life in volcanic mudpots. Environ Microbiol
467 16:255–264.
468 16. Hibi Y, Asai K, Arafuka H, Hamajima M, Iwama T, Kawai K. 2011. Molecular structure of La^{3+}-
469 induced methanol dehydrogenase-like protein in *Methylobacterium radiotolerans*. J Biosci
470 Bioeng 111:547–549.
471 17. Fitriyanto NA, Fushimi M, Matsunaga M, Pertiwiningrum A, Iwama T, Kawai K. 2011. Molecular
472 structure and gene analysis of Ce^{3+}-induced methanol dehydrogenase of *Bradyrhizobium* sp.
473 MAFF211645. J Biosci Bioeng 111:613–617.
474 18. Good NM, Vu HN, Suriano CJ, Subuyuj GA, Skovran E, Martinez-Gomez NC. 2016.
475 Pyrroloquinoline Quinone Ethanol Dehydrogenase in *Methylobacterium extorquens* AM1
476 Extends Lanthanide-Dependent Metabolism to Multicarbon Substrates. J Bacteriol 198:3109–

477 3118.
478 19. Vu HN, Subuyuj GA, Vijayakumar S, Good NM, Martinez-Gomez NC, Skovran E. 2016.
479 Lanthanide-Dependent Regulation of Methanol Oxidation Systems in *Methylobacterium*
480 *extorquens* AM1 and Their Contribution to Methanol Growth. J Bacteriol 198:1250–1259.
481 20. Masuda S, Suzuki Y, Fujitani Y, Mitsui R, Nakagawa T, Shintani M, Tani A. 2018. Lanthanide-
482 Dependent Regulation of Methylotrophy in *Methylobacterium aquaticum* Strain 22A. mSphere
483 3:e00462-17.
484 21. Chistoserdova L. 2016. Lanthanides: New life metals? World J Microbiol Biotechnol 32:138.
485 22. Keltjens JT, Pol A, Reimann J, Op den Camp HJM. 2014. PQQ-dependent methanol
486 dehydrogenases: rare-earth elements make a difference. Appl Microbiol Biotechnol 98:6163–
487 83.
488 23. Sowell SM, Abraham PE, Shah M, Verberkmoes NC, Smith DP, Barofsky DF, Giovannoni SJ. 2011.
489 Environmental proteomics of microbial plankton in a highly productive coastal upwelling
490 system. ISME J 5:856–865.
491 24. Taubert M, Grob C, Howat AM, Burns OJ, Dixon JL, Chen Y, Murrell JC. 2015. XoxF encoding an
492 alternative methanol dehydrogenase is widespread in coastal marine environments. Environ
493 Microbiol 17:3937–3948.
494 25. Lv H, Sahin N, Tani A. 2018. Isolation and genomic characterization of *Novimethylophilus*
495 *kurashikiensis* gen. nov. sp. nov., a new lanthanide-dependent methylotrophic species of
496 Methylophilaceae. Environ Microbiol 20:1204–1223.
497 26. Cotruvo JA, Featherston ER, Mattocks JA, Ho J V, Laremore TN. 2018. Lanmodulin: A Highly
498 Selective Lanthanide-Binding Protein from a Lanthanide-Utilizing Bacterium. J Am Chem Soc
499 jacs.8b09842.
500 27. Gu W, Semrau JD. 2017. Copper and cerium-regulated gene expression in *Methylosinus*
501 *trichosporium* OB3b. Appl Microbiol Biotechnol 101:8499–8516.
502 28. Good NM, Walser ON, Moore RS, Suriano CJ, Huff AF, Martinez-Gomez NC. 2018. Investigation
503 of lanthanide-dependent methylotrophy uncovers complementary roles for alcohol

504 dehydrogenase enzymes. bioRxiv 329011.

505 29. Fitriyanto NA, Nakamura M, Muto S, Kato K, Yabe T, Iwama T, Kawai K, Pertiwiningrum A. 2011.
506 Ce^{3+}-induced exopolysaccharide production by *Bradyrhizobium* sp. MAFF211645. J Biosci
507 Bioeng 111:146–152.

508 30. Zheng Y, Huang J, Zhao F, Chistoserdova L. 2018. Physiological Effect of XoxG(4) on Lanthanide-
509 Dependent Methanotrophy. MBio 9:e02430-17.

510 31. Krause SMB, Johnson T, Samadhi Karunaratne Y, Fu Y, Beck DAC, Chistoserdova L, Lidstrom ME.
511 2017. Lanthanide-dependent cross-feeding of methane-derived carbon is linked by microbial
512 community interactions. Proc Natl Acad Sci 114:358–363.

513 32. Akberdin IR, Collins DA, Hamilton R, Oshchepkov DY, Shukla AK, Nicora CD, Nakayasu ES, Adkins
514 JN, Kalyuzhnaya MG. 2018. Rare Earth Elements Alter Redox Balance in *Methylomicrobium*
515 *alcaliphilum* 20ZR. Front Microbiol 9:1–12.

516 33. Diatloff E, Smith FW, Asher CJ. 1995. Rare earth elements and plant growth: III. Responses of
517 corn and mungbean to low concentrations of cerium in dilute, continuously flowing nutrient
518 solutions. J Plant Nutr 18:1991–2003.

519 34. Diatloff E, Asher CJ, Smith FW. 1996. Rare earth elements and plant growth. Proc 8th Aust Agron
520 Conf Toowoomba, Queensland, Aust 30 January-2 February, 1996 3–6.

521 35. Pang X, Li D, Peng A. 2002. Application of rare-earth elements in the agriculture of China and
522 its environmental behavior in soil. Environ Sci Pollut Res 9:143–148.

523 36. Wahid PA, Valiathan MS, Kamalam N V., Eapen JT, Vijayalakshmi S, Prabhu RK, Mahalingam TR.
524 2000. Effect of rare earth elements on growth and nutrition of coconut palm and root
525 competition for these elements between the palm and *calotropis gigantea*. J Plant Nutr 23:329–
526 338.

527 37. Xie ZB, Zhu JG, Chu HY, Zhang YL, Zeng Q, Ma HL, Cao ZH. 2002. Effect of lanthanum on rice
528 production, nutrient uptake, and distribution. J Plant Nutr 25:2315–2331.

529 38. Wehrmann M, Berthelot C, Billard P, Klebensberger J. 2018. The PedS2/PedR2 Two-Component
530 System Is Crucial for the Rare Earth Element Switch in *Pseudomonas putida* KT2440. mSphere

531 3:1–12.

532 39. Farhan Ul Haque M, Kalidass B, Bandow N, Turpin EA, DiSpirito AA, Semrau JD. 2015. Cerium
533 Regulates Expression of Alternative Methanol Dehydrogenases in *Methylosinus trichosporium*
534 OB3b. Appl Environ Microbiol 81:7546–7552.

535 40. Chu F, Beck DAC, Lidstrom ME. 2016. MxaY regulates the lanthanide-mediated methanol
536 dehydrogenase switch in *Methylomicrobium buryatense*. PeerJ 4:e2435.

537 41. Ochsner AM, Hemmerle L, Vonderach T, Nüssli R, Bortfeld-Miller M, Hattendorf B, Vorholt JA.
538 2019. Use of rare-earth elements in the phyllosphere colonizer *Methylobacterium extorquens*
539 PA1. Mol Microbiol doi:10.1111/mmi.14208.

540 42. Chu F, Lidstrom ME. 2016. XoxF Acts as the Predominant Methanol Dehydrogenase in the Type
541 I Methanotroph *Methylomicrobium buryatense*. J Bacteriol 198:1317–1325.

542 43. Maniatis T, Fritsch E, Sambrook J, Laboratory CSH. 1982. Molecular Cloning : A Laboratory
543 Manual. Cold Spring Harbor, N.Y. Cold Spring Harbor Laboratory.

544 44. Kahm M, Kschischo M, Ludwig J, Lichtenberg-Fraté H, Hasenbrink G. 2015. grofit : Fitting
545 Biological Growth Curves with R . J Stat Softw 33.

546 45. Gibson DG. 2011. Enzymatic Assembly of Overlapping DNA Fragments, p. 349–361. *In* Methods
547 in Enzymology.

548 46. Graf N, Altenbuchner J. 2011. Development of a method for markerless gene deletion in
549 *Pseudomonas putida*. Appl Environ Microbiol 77:5549–5552.

550 47. Wessel D, Flügge UI. 1984. A method for the quantitative recovery of protein in dilute solution
551 in the presence of detergents and lipids. Anal Biochem 138:141–143.

552 48. Bradford MM. 1976. A rapid and sensitive method for the quantitation of microgram quantities
553 of protein utilizing the principle of protein-dye binding. Anal Biochem 72:248–254.

554 49. Rappsilber J, Ishihama Y, Mann M. 2003. Stop and Go Extraction Tips for Matrix-Assisted Laser
555 Desorption/Ionization, Nanoelectrospray, and LC/MS Sample Pretreatment in Proteomics. Anal
556 Chem 75:663–670.

557 50. de Godoy LMF, Mortensen P, Makarov A, Li G, Macek B, Horning S, Pesch R, Mann M, Olsen J

558 V., Lange O. 2005. Parts per Million Mass Accuracy on an Orbitrap Mass Spectrometer via Lock
559 Mass Injection into a C-trap. Mol Cell Proteomics 4:2010–2021.
560 51. Cox J, Mann M. 2008. MaxQuant enables high peptide identification rates, individualized p.p.b.-
561 range mass accuracies and proteome-wide protein quantification. Nat Biotechnol 26:1367–
562 1372.
563 52. Cox J, Neuhauser N, Michalski A, Scheltema RA, Olsen J V., Mann M. 2011. Andromeda: A
564 Peptide Search Engine Integrated into the MaxQuant Environment. J Proteome Res 10:1794–
565 1805.
566 53. Bateman A, Martin MJ, O'Donovan C, Magrane M, Alpi E, Antunes R, Bely B, Bingley M, Bonilla
567 C, Britto R, Bursteinas B, Bye-AJee H, Cowley A, Da Silva A, De Giorgi M, Dogan T, Fazzini F,
568 Castro LG, Figueira L, Garmiri P, Georghiou G, Gonzalez D, Hatton-Ellis E, Li W, Liu W, Lopez R,
569 Luo J, Lussi Y, MacDougall A, Nightingale A, Palka B, Pichler K, Poggioli D, Pundir S, Pureza L, Qi
570 G, Rosanoff S, Saidi R, Sawford T, Shypitsyna A, Speretta E, Turner E, Tyagi N, Volynkin V, Wardell
571 T, Warner K, Watkins X, Zaru R, Zellner H, Xenarios I, Bougueleret L, Bridge A, Poux S, Redaschi
572 N, Aimo L, ArgoudPuy G, Auchincloss A, Axelsen K, Bansal P, Baratin D, Blatter MC, Boeckmann
573 B, Bolleman J, Boutet E, Breuza L, Casal-Casas C, De Castro E, Coudert E, Cuche B, Doche M,
574 Dornevil D, Duvaud S, Estreicher A, Famiglietti L, Feuermann M, Gasteiger E, Gehant S, Gerritsen
575 V, Gos A, Gruaz-Gumowski N, Hinz U, Hulo C, Jungo F, Keller G, Lara V, Lemercier P, Lieberherr
576 D, Lombardot T, Martin X, Masson P, Morgat A, Neto T, Nouspikel N, Paesano S, Pedruzzi I,
577 Pilbout S, Pozzato M, Pruess M, Rivoire C, Roechert B, Schneider M, Sigrist C, Sonesson K, Staehli
578 S, Stutz A, Sundaram S, Tognolli M, Verbregue L, Veuthey AL, Wu CH, Arighi CN, Arminski L,
579 Chen C, Chen Y, Garavelli JS, Huang H, Laiho K, McGarvey P, Natale DA, Ross K, Vinayaka CR,
580 Wang Q, Wang Y, Yeh LS, Zhang J. 2017. UniProt: the universal protein knowledgebase. Nucleic
581 Acids Res 45:D158–D169.
582 54. Tyanova S, Temu T, Sinitcyn P, Carlson A, Hein MY, Geiger T, Mann M, Cox J. 2016. The Perseus
583 computational platform for comprehensive analysis of (prote)omics data. Nat Methods 13:731–
584 740.

585 55. Vizcaíno JA, Csordas A, Del-Toro N, Dianes JA, Griss J, Lavidas I, Mayer G, Perez-Riverol Y,
586 Reisinger F, Ternent T, Xu Q-W, Wang R, Hermjakob H. 2016. 2016 update of the PRIDE database
587 and its related tools. Nucleic Acids Res 44:D447–D456.
588 56. Galperin MY, Makarova KS, Wolf YI, Koonin E V. 2015. Expanded microbial genome coverage
589 and improved protein family annotation in the COG database. Nucleic Acids Res 43:D261–D269.
590 57. Nikel PI, Romero-Campero FJ, Zeidman J a, Goñi-Moreno Á, de Lorenzo V. 2015. The Glycerol-
591 Dependent Metabolic Persistence of *Pseudomonas putida* KT2440 Reflects the Regulatory Logic
592 of the GlpR Repressor. MBio 6:1–13.
593 58. Nikel PI, Kim J, de Lorenzo V. 2014. Metabolic and regulatory rearrangements underlying
594 glycerol metabolism in *Pseudomonas putida* KT2440. Environ Microbiol 16:239–254.
595 59. Walsh M, Casey M, Kenny S, Narancic T, Blank L, Wierckx N, Ballerstedt H, O'Connor KE. 2019.
596 Insights into an alternative pathway for glycerol metabolism in a glycerol kinase deficient
597 *Pseudomonas putida* KT2440. bioRxiv 567230.
598 60. Tessier FJ, Monnier VM, Sayre LM, Kornfield JA. 2003. Triosidines: novel Maillard reaction
599 products and cross-links from the reaction of triose sugars with lysine and arginine residues.
600 Biochem J 369:705–719.
601 61. Benov L, Beema AF. 2003. Superoxide-dependence of the short chain sugars-induced
602 mutagenesis. Free Radic Biol Med 34:429–433.
603 62. Li XZ, Zhang L, Poole K. 1998. Role of the multidrug efflux systems of *Pseudomonas aeruginosa*
604 in organic solvent tolerance. J Bacteriol 180:2987–91.
605 63. Hishinuma S, Yuki M, Fujimura M, Fukumori F. 2006. OxyR regulated the expression of two
606 major catalases, KatA and KatB, along with peroxiredoxin, AhpC in *Pseudomonas putida.*
607 Environ Microbiol 8:2115–2124.
608 64. Sigrist CJA, de Castro E, Cerutti L, Cuche BA, Hulo N, Bridge A, Bougueleret L, Xenarios I. 2012.
609 New and continuing developments at PROSITE. Nucleic Acids Res 41:D344–D347.
610 65. Agarwal N, Kalra VK. 1983. Interaction of lanthanide cations and uranyl ion with the
611 calcium/proton antiport system in *Mycobacterium phlei*. Biochim Biophys Acta - Biomembr

727:285–292.

66. Brown PH, Rathjen AH, Graham RD, Tribe DE. 1990. Chapter 92 Rare earth elements in biological systems, p. 423–452. *In* Handbook on the Physics and Chemistry of Rare Earths.

67. Peng L, Yi L, Zhexue L, Juncheng Z, Jiaxin D, Daiwen P, Ping S, Songsheng Q. 2004. Study on biological effect of La^{3+} on *Escherichia coli* by atomic force microscopy. J Inorg Biochem 98:68–72.

68. Mattocks JA, Ho J V., Cotruvo JA. 2019. A Selective, Protein-Based Fluorescent Sensor with Picomolar Affinity for Rare Earth Elements. J Am Chem Soc jacs.8b12155.

622 # Tables

623

624 **Table 1**: Specific enzyme activities of purified PedE and PedH with the four tested growth substrates
625 at 10 mM measured with 2,6-dichlorophenolindophenol (DCPIP) dependent colorimetric assay. Data
626 represent the average of biological triplicates with according standard deviation. Activities below
627 detection limit are indicated (n. d.).

628

Substrate	**Mean Specific Activity (U mg^{-1}) ± SD**	
	PedE 1 mM Ca^{2+}	**PedH 1 µM La^{3+}**
Citrate	n.d.	n.d.
Glucose	n.d.	n.d.
Glycerol	0.3 ± 0.1	0.9 ± 0.1
2-Phenylethanol	8.0 ± 0.4	6.3 ± 0.3

629

630 **Table 2**: Lag-times (λ), maximal OD_{600} during stationary phase (OD_{600}^{max}), and maximal growth rates
631 (μ_{max}) of different *P. putida* strains during growth with M9 medium supplemented with 20 mM glycerol
632 and 0 µM or 10 µM La^{3+} incubated in microtiter plates at 30°C and 250 rpm (see also Fig. 2 and Fig.5).
633 Maximal growth rates and lag-times were determined by fitting growth curves to the Richards model
634 using "grofit" package in R (44). Cultures were incubated at 250 rpm and 30°C in microplate reader
635 with constant OD_{600} measurement. Data points represent average of biological triplicates with
636 corresponding error (λ, μ_{max}) or standard deviation (OD_{600}^{max}). No growth parameters could be
637 determined for cultures that did not reach stationary phase during incubation time (n. d.).
638

Strain	**λ [h]**		**OD_{600}^{max}**		**μ_{max} [h^{-1}]**	
	0 µM La^{3+}	**10 µM La^{3+}**	**0 µM La^{3+}**	**10 µM La^{3+}**	**0 µM La^{3+}**	**10 µM La^{3+}**
KT2440*	17.3 ± 0.2	10.2 ± 0.2	0.884 ± 0.004	0.680 ± 0.014	0.341 ± 0.010	0.201 ± 0.004
Δ*pedE* Δ*pedH*	17.5 ± 0.3	17.2 ± 0.4	0.869 ± 0.002	0.802 ± 0.013	0.276 ± 0.008	0.291 ± 0.012
Δ*garK*	17.1 ± 0.3	n.d.	0.805 ± 0.005	n.d.	0.321 ± 0.011	n.d.
Δ*calA*	16.0 ± 0.3	11.1 ± 0.3	0.890 ± 0.004	0.753 ± 0.006	0.336 ± 0.011	0.271 ± 0.008
Δ*glcDEF*	17.0 ± 0.2	10.1 ± 0.2	0.862 ± 0.016	0.678 ± 0.004	0.315 ± 0.009	0.207 ± 0.004

639

640 **Table 3:** List of regulated proteins in presence of 10 µM La^{3+} compared to the absence of La^{3+} when
641 grown with glycerol as sole C-source.
642

Locus Tag	Protein name	Fold change induction (log_2)	- log_{10}(*p*-value)
PP_2426	CalA	6.28	4.03
PP_2679	PedH	4.75	3.80
PP_3426	MexF	3.93	3.24
PP_3425	MexE	3.74	2.18
PP_4921		3.65	2.46
PP_2440	AhpF	3.13	3.08
PP_3745	GlcD	3.12	3.32
PP_3747	GlcF	2.67	3.50
PP_3746	GlcE	2.64	2.98
PP_4922	ThiC	2.21	3.84
PP_3748	GlcG	2.06	3.71
PP_3622		1.97	2.82
PP_3178	GarK	1.77	2.85
PP_3621	IorA-II	1.60	2.34
PP_0554	AcoB	1.54	2.27
PP_3623	AdhB	1.54	3.67
PP_2484		1.52	2.37
PP_0734	HemK	1.51	2.67
PP_2439	AhpC	1.39	2.02
PP_0556		1.35	2.34
PP_1125		1.30	3.01
PP_0555	AcoA	1.20	2.52
PP_1548		1.19	2.03
PP_1351	PanE	-1.45	2.06
PP_2258		-1.84	2.40
PP_5658		-1.99	2.93
PP_3557		-2.41	2.33
PP_3603		-2.46	2.73
PP_4313		-2.55	2.50
PP_0588		-2.75	2.62
PP_2674	PedE	-4.25	3.78
PP_2673		-5.37	3.71
PP_3732		-5.78	3.07

643

644 **Table S1:** Strains and plasmids used in the study

645

Strains	**Relevant features**	**Source or reference**
KT2440*	KT2440 with a markerless deletion of *upp* | Parent strain for deletion mutants	(46)
Δ*pedE*	KT2440* with a markerless deletion of *pedE*	(11)
Δ*pedH*	KT2440* with a markerless deletion of *pedH*	(11)
Δ*calA*	KT2440* with a markerless deletion of *calA*	this study
Δ*garK*	KT2440* with a markerless deletion of gene *garK*	this study
Δ*glcDEF*	KT2440* with a markerless deletion of gene cluster *glcDEF*	this study
Δ*pedE* Δ*pedH*	KT2440* with a markerless deletion of *pedE and pedH*	(11)
Δ*pedE* Δ*pedH* Δ*glpFKRD*	Δ*pedE*Δ*pedH* with a markerless deletion of gene cluster Δ*glpFKRD*	this study
E. coli TOP10	*F- mcrA Δ(mrr-hsdRMS-mcrBC) φ80lacZΔM15 ΔlacX74 nupG recA1 araD139 Δ(ara-leu)7697 galE15 galK16 rpsL(Str^R) endA1 λ$^-$*	Invitrogen
Plasmids		
pJOE6261.2	Suicide vector for gene deletions	(46)
pJOE-calA	pJOE6261.2 based deletion vector for gene *calA* (PP_2426)	this study
pJOE-garK	pJOE6261.2 based deletion vector for gene *garK* (PP_3178)	this study
pJOE-glp	pJOE6261.2 based deletion vector for gene cluster *glpFKRD* (PP_1076 to PP_1073)	this study
pMW08	pJOE6261.2 based deletion vector for gene cluster *glcDEF* (PP_3745 to PP_3747)	this study

646

647 **Table S2:** Primers used in the study

648

Primer		
Name	**Sequence 5' → 3'**	**Annealing temperature**
PcalA1	CGATGGCCGCTTTGGTCCCGAGCCGTTCCACACTTTCGC	67°C
PcalA2	AACCGATCAAGCAGGGCCTCGCAGTGAA	67°C
PcalA3	GAGGCCCTGCTTGATCGGTTGCCTGTACG	65°C
PcalA4	CCTGCAGGTCGACTCTAGAGCGTGGGTGAGCAAGGCAG	65°C
PgarK1	CGATGGCCGCTTTGGTCCCGAGTCGTTGCTGTGGTGCC	62°C
PgarK2	TACAGGGTGTGGGGTTTCTCCTGTCCTG	62°C
PgarK3	GAGAAACCCCACACCCTGTAGAAATGGCCTTATTG	67°C
PgarK4	CCTGCAGGTCGACTCTAGAGCAGCGGCAAACTGACCATC	67°C
Pglp1	CGATGGCCGCTTTGGTCCCGGTCATCAATAAAGGTCCG	55°C
Pglp2	ACCGTAGGTAGTATGACCTCGTTTTTTTTG	55°C
Pglp3	GAGGTCATACTACCTACGGTGAAGCCCTC	62°C
Pglp4	CCTGCAGGTCGACTCTAGAGGTTGTGAAGACCGCCTGC	62°C
MWH03	AGGCACGATGGCCGCTTTGGTCCCGGCCTGCTCGGGCAGTTGTTCC	63°C
MWH04	GCTAAGCATGGGCCATCGGCTCACTCGCAAC	63°C
MWH05	AGTGAGCCGATGGCCCATGCTTAGCAAGTTCGTTATCG	63°C
MWH06	GCATGCCTGCAGGTCGACTCTAGAGCCAGGGCAATGCGTATCAC	63°C

649

650 **Table S3:** List of regulated proteins in presence of 10 µM La^{3+} compared to the absence of La^{3+} when
651 grown with 2-phenylethanol as sole C-source.
652

Locus Tag	Protein name	Fold change induction (log_2)	- log_{10}(*p*-value)
PP_2679	PedH	3.41	2.48
PP_3357	Vdh	2.65	2.92
PP_5125	MutM	2.24	3.15
PP_4905	MotA	1.84	2.01
PP_0091		1.71	2.26
PP_5157		1.59	2.20
PP_0342	WaaC	1.43	2.46
PP_3722	Alr	1.04	2.40
PP_2674	PedE	-1.49	5.90
PP_2673		-2.41	3.91

653

654 **Table S4:** List of regulated proteins in presence of 10 µM La^{3+} compared to the absence of La^{3+} when
655 grown with glucose as sole C-source.
656

Locus Tag	Protein name	Fold change induction (log_2)	- log_{10}(*p*-value)
PP_2679	PedH	4.35	3.17
PP_4508		1.74	2.97
PP_3713	CatA	1.44	2.43
PP_5221		1.39	2.21
PP_0367		1.27	2.47
PP_4796	HolA	-1.30	2.15
PP_4374	FliT	-1.95	2.45
PP_2666		-2.01	2.51
PP_3951	PcaI	-2.13	2.68
PP_2680	AldB-II	-2.79	2.41
PP_4632	FolM	-3.54	2.53
PP_2662		-3.61	3.62
PP_1757	BolA	-3.64	3.99
PP_2674	PedE	-6.97	4.13

657

658 **Table S5:** List of regulated proteins in presence of 10 µM La^{3+} compared to the absence of La^{3+} when
659 grown with citrate as sole C-source.
660

Locus Tag	Protein name	Fold change induction (log_2)	- log_{10}(*p*-value)
PP_2491		2.27	4.32
PP_0365	BioC	1.12	2.06
PP_4157	KdpE	-1.41	2.72
PP_2674	PedE	-2.56	2.80
PP_0634	PilA	-3.08	3.88

661

662 **Figures**

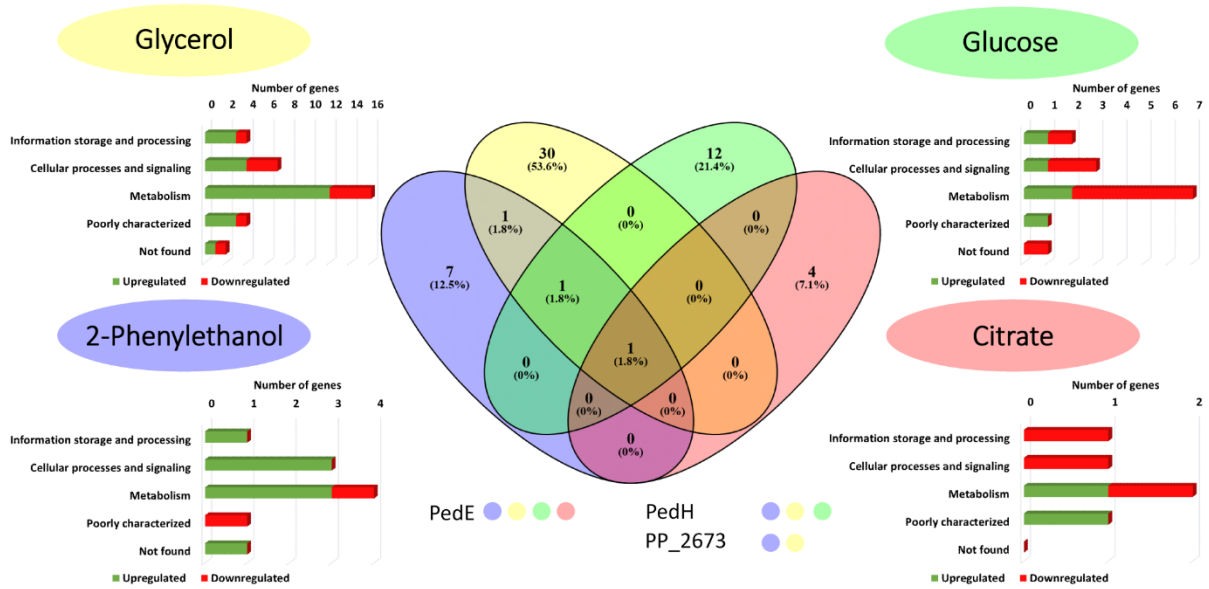

663
664
665 **Figure 1**: Venn-diagram (middle) of differentially produced proteins in response to 10 µM La^{3+} during
666 growth with glycerol, glucose, 2-phenylethanol and citrate. Proteins that showed up under several
667 growth conditions are stated under the diagram with colour code for classification (yellow dot =
668 glycerol; green dot = glucose; blue dot = 2-phenylethanol; red dot = citrate). Classifications of
669 differentially expressed proteins according to the Cluster of Orthologous Groups database are depicted
670 for each substrate.
671

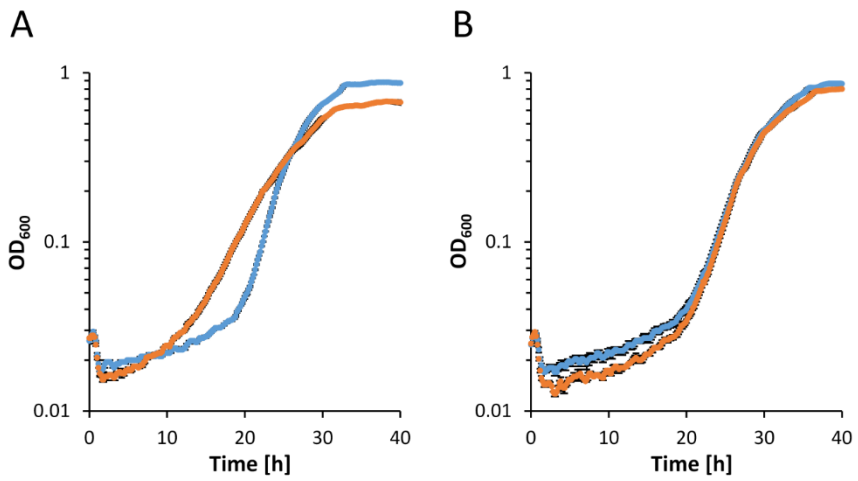

Figure 2: Growth of strains (**A**) KT2440* and (**B**) Δ*pedE* Δ*pedH* in M9 minimal medium supplemented with 20 mM glycerol in the absence (blue dots) or presence of 10 µM La^{3+} (orange dots) in 96-well microtiter plates at 30°C and 250 rpm. Data represent average of biological triplicates with corresponding standard deviation.

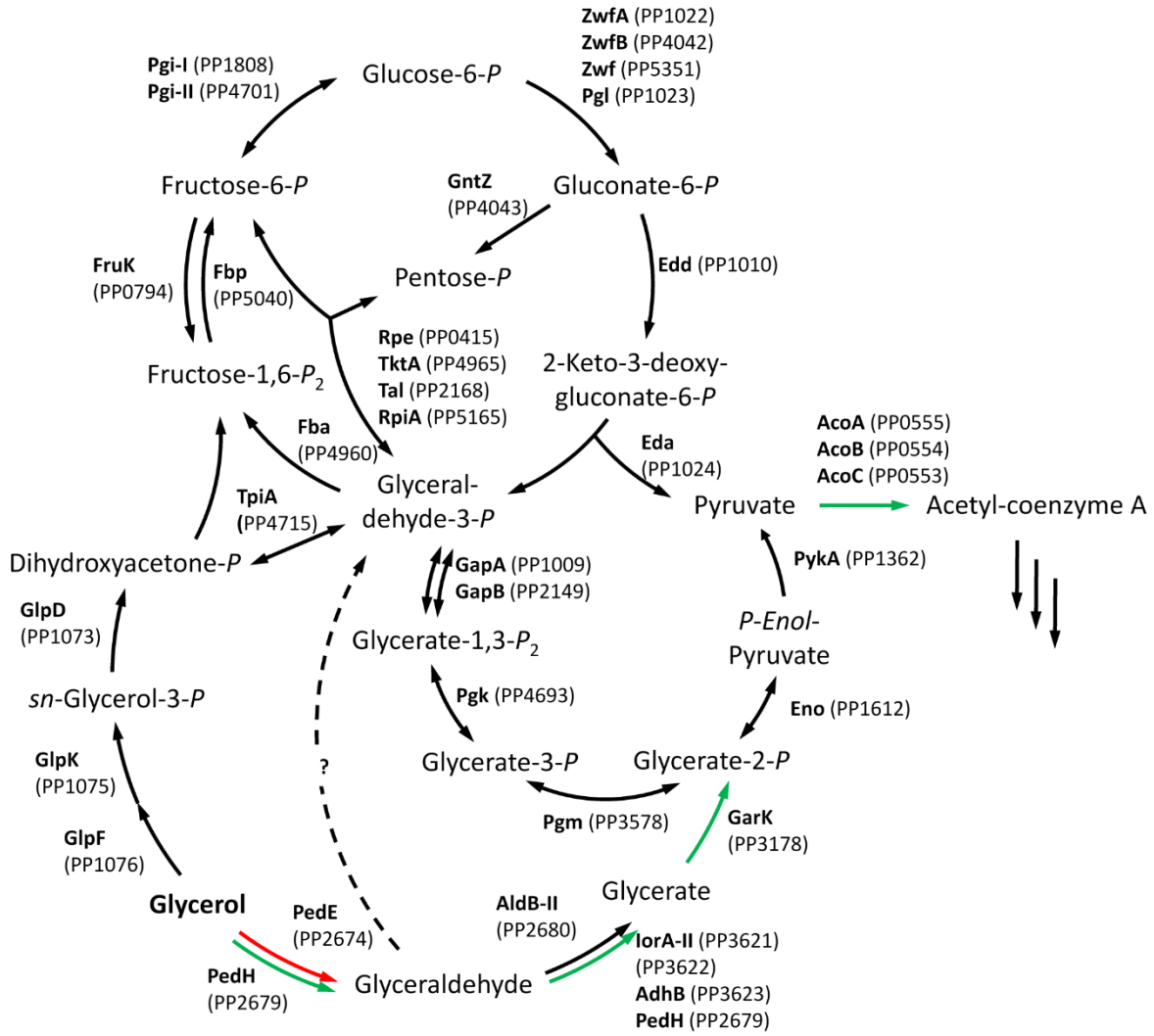

Figure 3: Proteins of the upstream central carbon metabolism of *P. putida* KT2440 including the proposed glycerol degradation pathway via glycerate and the additional hypothetical route through phosphorylation of glyceraldehyde (dotted line). Anticipated metabolic flux by the proteins that were identified as differentially abundant in response to 10 µM La^{3+} during growth on glycerol are colour-coded (green = increased, red = decreased, black = not affected). The figure is inspired by a scheme originally published by Nikel *et al.* (58) and was adapted to include the novel metabolic route(s) identified in this study.

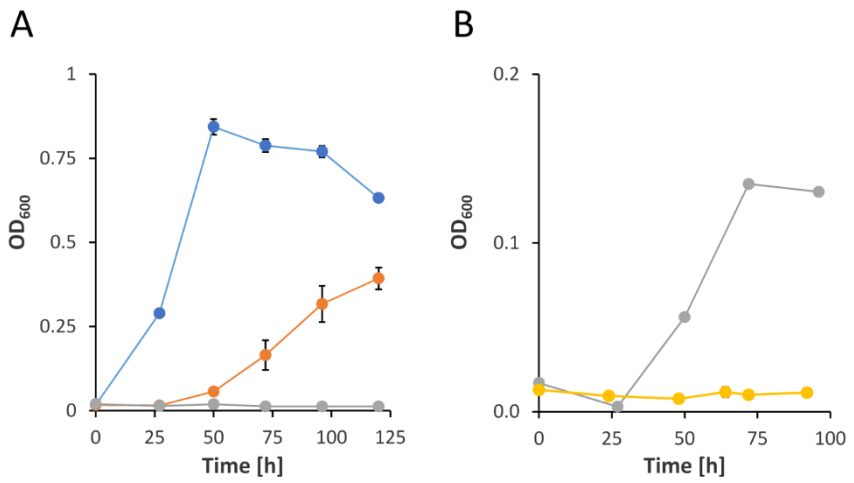

Figure 4: (**A**) Growth of strains Δ*pedE* Δ*pedH* (blue dots), Δ*glpFKRD* (orange dots), and Δ*pedE* Δ*pedH* Δ*glpFKRD* (grey dots) in M9 minimal medium supplemented with 20 mM glycerol in 96-well microtiter plates. (**B**) Growth of strains Δ*pedE* Δ*pedH* Δ*glpFKRD* (grey dots) and Δ*garK* (yellow dots), in M9 minimal medium supplemented with 20 mM DL-glycerate incubated in 96-well microtiter plates at 28°C and 220 rpm. Data represent average of biological triplicates with corresponding standard deviation.

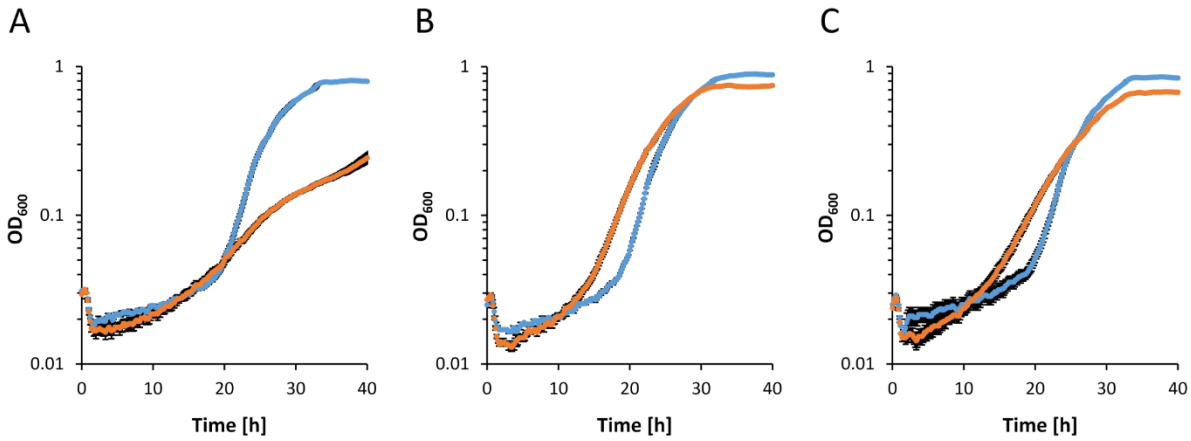

Figure 5: Growth of strains (**A**) Δ*garK,* (**B**) Δ*calA*, and (**C**) Δ*glcDEF* in M9 minimal medium supplemented with 20 mM glycerol in absence (blue dots) or presence 10 µM La^{3+} (orange dots) incubated in 96-well microtiter plates at 30°C and 250 rpm. Data represent average of biological triplicates with corresponding standard deviation.

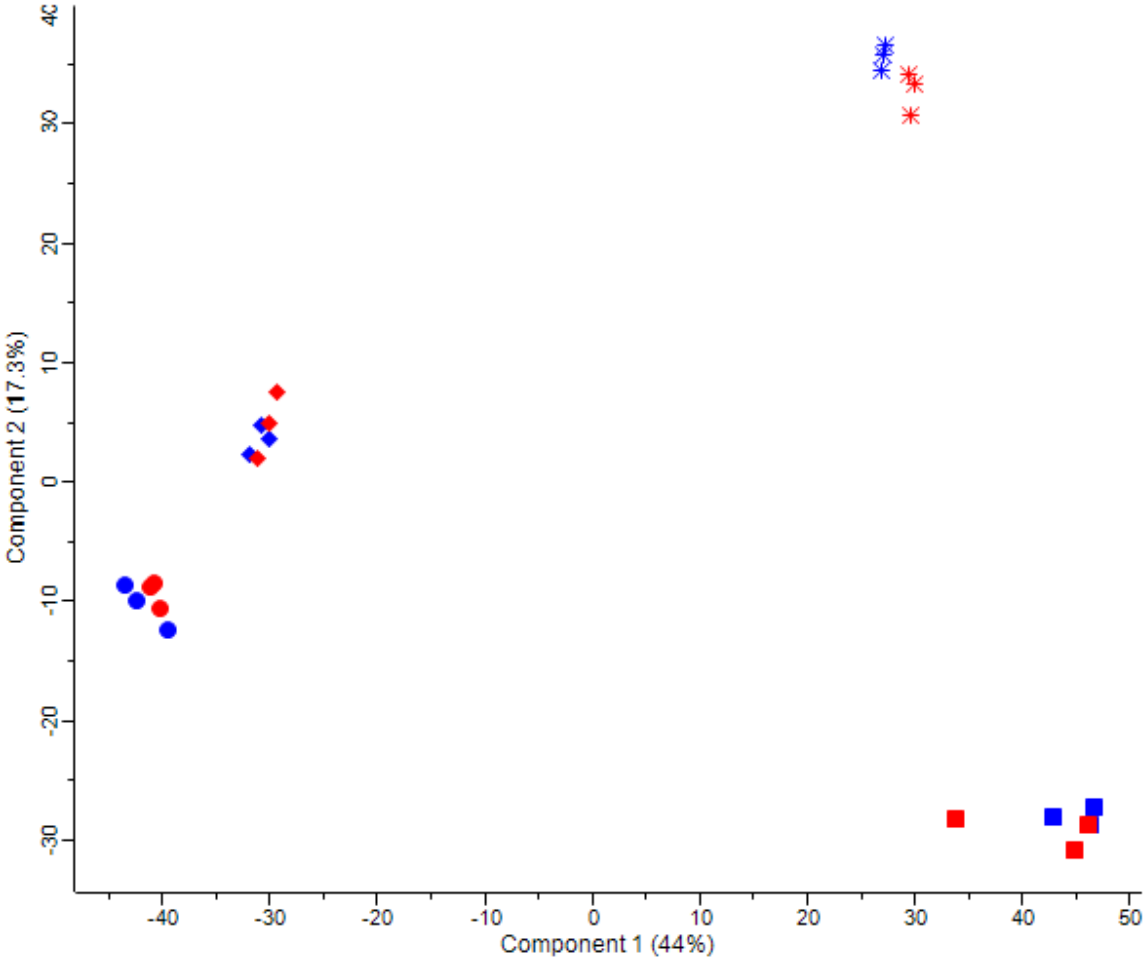

705

706 **Figure S1**: **PCA comparing the four different carbon sources with and without La^{3+}.** Different carbon
707 sources are indicated by squares (2-phenylethanol), circles (citrate), diamonds (glucose) and stars
708 (glycerol). Samples with 10 µM La^{3+} or without La^{3+} in the medium are shown in blue and red,
709 respectively. Biological replicates are indicated in the same colour. Samples can be separated
710 according to different carbon sources while treatment with La^{3+} only showed minor effects.